Check for updates

RESEARCH ARTICLE

WILEY

High order accurate and convergent numerical scheme for the strongly anisotropic Cahn–Hilliard model

Kelong Cheng[1] | Cheng Wang[2] | Steven M. Wise[3]

[1]School of Science, Civil Aviation Flight University of China, Guanghan, Sichuan, People's Republic of China
[2]Department of Mathematics, The University of Massachusetts, North Dartmouth, Massachusetts, USA
[3]Department of Mathematics, The University of Tennessee, Knoxville, Tennessee, USA

Correspondence
Steven M. Wise, Department of Mathematics, The University of Tennessee, Knoxville, TN 37996, USA.
Email: swise1@utk.edu

Abstract

We propose and analyze a second order accurate in time, energy stable numerical scheme for the strongly anisotropic Cahn–Hilliard system, in which a biharmonic regularization has to be introduced to make the equation well-posed. A convexity analysis on the anisotropic interfacial energy is necessary to overcome an essential difficulty associated with its highly nonlinear and singular nature. The second order backward differentiation formula temporal approximation is applied, combined with Fourier pseudo-spectral spatial discretization. The nonlinear surface energy part is updated by an explicit extrapolation formula. Meanwhile, the energy stability analysis is enforced by the fact that all the second order functional derivatives of the energy stay uniformly bounded by a global constant. A Douglas-Dupont type regularization is added to stabilize the numerical scheme, and a careful estimate ensures a modified energy stability with a uniform constraint for the regularization parameter A. In turn, the combination with an appropriate treatment for the nonlinear double well potential terms leads to a weakly nonlinear scheme. More importantly, such an energy stability is in terms of the interfacial energy with respect to the original phase variable, which enables us to derive an optimal rate convergence analysis.

1 | INTRODUCTION

The Cahn–Hilliard equation has been a very well-known gradient flow, modeling spinodal decomposition and phase separation in a binary alloy [5,6]. A prominent advantage of this model, narrow diffusive transition layers replace sharp interfaces, so that a theoretical analysis of the equation becomes more feasible than the sharp interface counterparts. In addition, the phase field model shows great advantage over the sharp interface counterpart if the surface energy density is a smooth function of the interface normal and the anisotropy becomes sufficiently strong. In such a case, the Wulff shape (the shape that minimizes the total surface energy for a given volume [7,47]) may have missing orientations. Regularizing the sharp interface model to avoid discontinuity requires a complicated highly nonlinear term that depends upon the curvature [37]. Nonetheless, strong anisotropy plays important roles in the material properties of heterogeneous solids, and efficient, stable, and accurate numerical simulations are required.

In this article, we focus on the strongly anisotropic Cahn–Hilliard model over a bounded domain $\Omega \subset \mathbb{R}^d$, $d = 2, 3$. The phase variable is given by ϕ, and its gradient vector is denoted as $\boldsymbol{p} := \nabla\phi$, for simplicity of presentation. In turn, the unit normal vector $\boldsymbol{n} := \frac{\boldsymbol{p}}{|\boldsymbol{p}|}$ (with respect to iso-contours of ϕ) has the following components, which is well-defined for any non-zero vector $\nabla\phi$:

$$n_i = \frac{\partial_{x_i}\phi}{|\nabla\phi|} = \frac{p_i}{|\boldsymbol{p}|}, \quad i = 1, \dots, d.$$

The strongly anisotropic, Kobayashi-type free energy [40] free energy is formulated as

$$E(\phi) = \int_\Omega \left(f(\phi) + \frac{\varepsilon^2}{2}\gamma^2(\boldsymbol{n})|\boldsymbol{p}|^2 + \beta\frac{\varepsilon^2}{2}(\Delta\phi)^2 \right) d\boldsymbol{x}, \quad f(\phi) = \frac{1}{4}(\phi^2 - 1)^2, \quad \gamma(\boldsymbol{n}) = 1 + \alpha\Gamma(\boldsymbol{n}), \quad (1.1)$$

where $\varepsilon > 0$, $\beta \geq 0$, and $\alpha \geq 0$ stand for the interface transition width parameter, an anisotropy regularization parameter (sometimes called a corner-rounding parameter), and the anisotropy strength, respectively, and $\gamma(\boldsymbol{n})$ models the anisotropy in the interfacial energy function. The inclusion of the higher order regularization term avoids the well-known difficulty associated with the possibility of ill-posedness in the strong anisotropy regime due to a sign change of the surface stiffness [4,22,50,54]. Various options are available, including the simple bi-harmonic regularization [54] or the nonlinear Willmore regularization [10,41,42,44,45,51]. A completely new formulation that uses the Willmore regularization can be found in [46]. From the computational standpoint, at least, it is clear that the biharmonic regularization is simpler, though the Willmore has better asymptotic properties. See the relevant discussions in [51,53,54].

In the case of four-fold anisotropy, the anisotropy structure function $\Gamma(\boldsymbol{n})$ takes the form as

$$\Gamma(\boldsymbol{n}) = \Gamma_4(\boldsymbol{n}) := 4\sum_{i=1}^d n_i^4 - 3. \quad (1.2)$$

An extension of the analysis to more exotic forms of anisotropy, such as the eight-fold version, is be straightforward, as will be demonstrated in later sections. If $\alpha > 0$ is sufficiently large, missing orientations appear on the Wulff shape. Without regularization, discontinuities in the derivatives of ϕ appear, and the PDE model may no longer be well-posed.

For the sake of convenience, we assume periodic boundary condition in this article. The H^{-1} gradient flow of the anisotropic Cahn–Hilliard energy is

$$\partial_t \phi = \Delta \mu, \quad \mu = \phi^3 - \phi - \varepsilon^2 \nabla \cdot \left(\gamma^2(\boldsymbol{n}) \nabla \phi + \gamma(\boldsymbol{n}) |\nabla \phi| \mathbf{P} \nabla_n \gamma(\boldsymbol{n}) \right) + \beta \varepsilon^2 \Delta^2 \phi, \qquad (1.3)$$

where ∇_n is the gradient with respect to $\boldsymbol{n}$, and $\mathbf{P} := \mathbf{I} - \boldsymbol{n} \otimes \boldsymbol{n}$, is the interface projection matrix, and $\mathbf{I}$ is the identity matrix.

Many numerical works have reported interesting computational results for the anisotropic Cahn–Hilliard equation, including [10,26,43,54], to name a few. Meanwhile, a theoretical justification of the energy stability has always very challenging issue, due to the highly singular nature of the surface energy. Among the existing works to address this issue, a convex splitting approach is applied to the anisotropic system with a Willmore regularization in [14], while a theoretical proof for the energy stability is only available for the isotropic flow. A stabilized scalar auxiliary variable (SAV) approach is studied in [9,56], and a stability analysis has been provided for a numerically modified energy. On the other hand, a uniform in time bound for the original energy functional (1.1) (in terms of the original phase variable) is not theoretically available in this approach, so that a convergence analysis would face serious difficulty. In addition, it is worthy of mentioning a recent work [20], in which a convexity analysis is performed for the anisotropic surface energy part, so that an explicit treatment could be applied to the corresponding chemical potential, combined with a first order regularization. In turn, an energy stability is derived for the corresponding numerical scheme, and the numerical algorithm is only weakly nonlinear, in the sense that the nonlinearity only appears in the double well energy potential part.

Of course, the direct application of linear convex splitting leads to only first order accurate (in time) numerical schemes, similar to the one reported in [11] for the no-slope-selection epitaxial thin film growth model. In this article, we propose and analyze second order accurate, energy stable numerical schemes for the anisotropic Cahn–Hilliard system, with the stability in terms of the original energy functional (1.1). The standard second order backward differential formula (BDF2) temporal stencil is applied, with all the chemical potential terms evaluated or approximated at time step t^{n+1}. This is combined with the Fourier pseudo-spectral spatial approximation. To overcome a well-known difficulty associated with the highly nonlinear nature in the chemical potential of the surface energy part, we recall a convexity analysis for $\gamma(\boldsymbol{n})$, which reveals that all its second order functional derivatives stay uniformly bounded by a global constant. As a result of this convexity analysis, we are able to approximate the nonlinear surface energy parts by an explicit extrapolation formula, combined with a second order accurate Douglas-Dupont type regularization, in the form of $-As\Delta_N(\phi^{n+1} - \phi^n)$. Since all the second order functional derivatives of the nonlinear surface diffusion part have a uniform bound, a theoretical justification of the energy stability becomes available, under a constraint for the artificial regularization parameter. Furthermore, such an energy stability is in terms of the original phase variable, and no auxiliary variable needs to be introduced. This approach avoids an implicit treatment of the nonlinear surface energy part, so that computational efficiency can be greatly improved.

In addition, we perform an optimal rate convergence analysis for the proposed second order numerical scheme for the anisotropic Cahn–Hilliard system. In this analysis, the global bound for the second order functional derivatives will also play an important role. This is the first such result for the second order scheme for the anisotropic Cahn–Hilliard model, to the best of our knowledge.

This article is organized as follows. In Section 2, we review a convexity analysis for the surface diffusion coefficients. The fully discrete numerical scheme for the strongly anisotropic system is considered in Section 3, with Fourier pseudo-spectral spatial discretization. The unique solvability and energy stability are theoretically justified. Moreover, an optimal rate convergence analysis is presented in Section 4. Some numerical results are presented in Section 5, and concluding remarks are made in Section 6.

2 | REVIEW OF THE CONVEXITY ANALYSIS FOR THE SURFACE ENERGY

The highly singular and nonlinear nature of $\gamma(\boldsymbol{n})$ is a key difficulty for the anisotropic model. As stated earlier, we focus on the four-fold anisotropy function

$$\gamma(\boldsymbol{n}) = 1 - 3\alpha + 4\alpha(n_1^4 + n_2^4 + n_3^4), \quad 0 \leq \alpha < \frac{3}{5} =: \alpha_1.$$

The minimum of $\gamma(\boldsymbol{n})$ occurs for $n_1^2 = n_2^2 = n_3^2 = \frac{1}{3}$, and we observe that $\gamma(\boldsymbol{n}) \leq 0$ for some orientations $\boldsymbol{n}$ if $\alpha \geq \alpha_1$. Thus, $\alpha_1 = \frac{3}{5}$ can be considered a critical value of α. The eight-fold anisotropy function would be treated similarly, though the precise details will differ.

For the four-fold function, a detailed expansion reveals that

$$\gamma^2(\boldsymbol{n}) = (1 - 3\alpha)^2 + 8\alpha(1 - 3\alpha)\frac{p_1^4 + p_2^4 + p_3^4}{(p_1^2 + p_2^2 + p_3^2)^2} + 16\alpha^2 \frac{(p_1^4 + p_2^4 + p_3^4)^2}{(p_1^2 + p_2^2 + p_3^2)^4}. \tag{2.1}$$

This yields

$$\mathcal{G}(\boldsymbol{p}) = \gamma^2(\boldsymbol{n})|\boldsymbol{p}|^2 = (1 - 3\alpha)^2|\boldsymbol{p}|^2 + 8\alpha(1 - 3\alpha)g^{(1)}(\boldsymbol{p}) + 16\alpha^2 g^{(2)}(\boldsymbol{p}), \tag{2.2}$$

$$g^{(1)}(\boldsymbol{p}) := \frac{p_1^4 + p_2^4 + p_3^4}{p_1^2 + p_2^2 + p_3^2}, \quad g^{(2)}(\boldsymbol{p}) := \frac{(p_1^4 + p_2^4 + p_3^4)^2}{(p_1^2 + p_2^2 + p_3^2)^3}. \tag{2.3}$$

In more details, the first order derivatives of $g^{(1)}$ and $g^{(2)}$ become

$$\partial_{p_i} g^{(1)}(\boldsymbol{p}) = \frac{4p_i^3 \sum_{j=1}^3 p_j^2 - 2p_i \sum_{j=1}^3 p_j^4}{\left(\sum_{j=1}^3 p_j^2\right)^2}, \quad i = 1, 2, 3, \tag{2.4}$$

$$\partial_{p_i} g^{(2)}(\boldsymbol{p}) = \frac{2p_i \sum_{j=1}^3 p_j^4 \left(4p_i^2 \sum_{j=1}^3 p_j^2 - 3\sum_{j=1}^3 p_j^4\right)}{\left(\sum_{j=1}^3 p_j^2\right)^4}, \quad i = 1, 2, 3. \tag{2.5}$$

The following preliminary estimates are excerpted from a recent work [20]; they will be useful in the energy theoretical analyses.

Lemma 2.1 ([20]). *Define*

$$D_1^{(1)} := \frac{7}{2}, \quad D_2^{(1)} := 2, \quad D_1^{(2)} := 6, \quad D_2^{(2)} := 3.$$

The functions $g^{(1)}$, $g^{(2)}$, are twice continuously differentiable in $\mathbb{R}^3_\star := \mathbb{R}^3 \setminus \{\mathbf{0}\}$, and

$$|\partial^2_{p_i} g^{(1)}(\mathbf{p})| \le D_1^{(1)}, \quad i = 1, 2, 3, \qquad |\partial_{p_i} \partial_{p_j} g^{(1)}(\mathbf{p})| \le D_2^{(1)}, \quad i, j = 1, 2, 3, \ i \ne j, \quad (2.6)$$

$$|\partial^2_{p_i} g^{(2)}(\mathbf{p})| \le D_1^{(2)}, \quad i = 1, 2, 3, \qquad |\partial_{p_i} \partial_{p_j} g^{(2)}(\mathbf{p})| \le D_2^{(2)}, \quad i, j = 1, 2, 3, \ i \ne j, \quad (2.7)$$

for all $\mathbf{p} \in \mathbb{R}^3_\star$. In addition, for any $\mathbf{p}_1, \mathbf{p}_2 \in \mathbb{R}^3$, we have

$$\left| \partial_{p_i} g^{(k)}(\mathbf{p}_1) - \partial_{p_i} g^{(k)}(\mathbf{p}_2) \right| \le \left(D_1^{(k)} - D_2^{(k)} \right) |q_i| + D_2^{(k)} \sum_{j=1}^{3} |q_i|, \quad k = 1, 2, \quad i = 1, 2, 3, \quad (2.8)$$

with $D_1^{(1)} = \frac{7}{2}, D_2^{(1)} = 2, D_1^{(2)} = 6, D_2^{(2)} = 3$, and $\mathbf{q} := \mathbf{p}_2 - \mathbf{p}_1$.

To obtain a linear numerical scheme for the anisotropic model, we rewrite the surface free energy as follows, which comes from the expansion for $\mathcal{G}(\mathbf{p}) = \gamma^2(\mathbf{n})|\mathbf{p}|^2$ in (2.1)–(2.3):

$$E_S(\phi) := \int_\Omega \mathcal{G}(\mathbf{p}) \, d\mathbf{x} = (1 - 3\alpha)^2 \|\nabla\phi\|^2 + E_{S,1}(\phi), \quad (2.9)$$

$$E_{S,1}(\phi) := \int_\Omega \left(8\alpha(1 - 3\alpha)g^{(1)}(\mathbf{p}) + 16\alpha^2 g^{(2)}(\mathbf{p}) \right) d\mathbf{x}, \quad \mathbf{p} = \nabla\phi. \quad (2.10)$$

In turn, the following functional is introduced

$$H_2(\phi) := A_2 \|\nabla\phi\|^2 - E_{S,1}(\phi) = \int_\Omega \left(A_2 |\mathbf{p}|^2 - 8\alpha(1 - 3\alpha)g^{(1)}(\mathbf{p}) - 16\alpha^2 g^{(2)}(\mathbf{p}) \right) d\mathbf{x}. \quad (2.11)$$

Therefore, the original energy (1.1) can be decomposed variously as

$$\begin{aligned}
E(\phi) &= (f(\phi), 1) + \frac{\varepsilon^2}{2} E_S(\phi) + \beta \frac{\varepsilon^2}{2} \|\Delta\phi\|^2 \\
&= (f(\phi), 1) + \frac{\varepsilon^2}{2}(1 - 3\alpha)^2 \|\nabla\phi\|^2 + \frac{\varepsilon^2}{2} E_{S,1}(\phi) + \beta \frac{\varepsilon^2}{2} \|\Delta\phi\|^2 \\
&= (f(\phi), 1) + \frac{\varepsilon^2}{2} \left[(1 - 3\alpha)^2 + A_2 \right] \|\nabla\phi\|^2 - \frac{\varepsilon^2}{2} H_2(\phi) + \beta \frac{\varepsilon^2}{2} \|\Delta\phi\|^2. \quad (2.12)
\end{aligned}$$

In addition, the following convexity result is available.

Proposition 2.2 ([20]). *The functional $H_2(\phi)$ is convex on $\mathbb{R}^3_\star$ provided that*

$$A_2 \ge A_2^\star := 8\alpha^2 A_0 + 4\alpha|1 - 3\alpha|B_0, \quad (2.13)$$

where

$$A_0 = 12 \quad \text{and} \quad B_0 = \frac{15}{2}. \quad (2.14)$$

Remark 2.3. For the remainder of the article, we will assume that $A_2 = A_2^\star$ in the definition of H_2. For $A_2 \ge A_2^\star$, the convexity of H_2 is still ensured, while a larger value of A_2 may bring more numerical diffusion, so that we prefer $A_2 = A_2^*$.

To facilitate the notation, we represent the variational derivative of $E_{S,1}$ as

$$\delta_\phi E_{S,1} = -\nabla \cdot \left((\gamma^2(\mathbf{n}) - (1 - 3\alpha)^2)\nabla\phi + \gamma(\mathbf{n})|\nabla\phi| \mathbf{P} \nabla_n \gamma(\mathbf{n}) \right). \quad (2.15)$$

Moreover, a more detailed expansion of this term is needed in the later derivation, based on the expansion in (2.1)–(2.3):

$$\delta_\phi E_{S,1} = -\nabla \cdot \left(8\alpha(1-3\alpha)\nabla_p g^{(1)}(\boldsymbol{p}) + 16\alpha^2 \nabla_p g^{(2)}(\boldsymbol{p})\right)$$

$$= -\nabla \cdot \left(8\alpha(1-3\alpha)\begin{pmatrix}\partial_{p_1} g^{(1)}(\boldsymbol{p}) \\ \partial_{p_2} g^{(1)}(\boldsymbol{p}) \\ \partial_{p_3} g^{(1)}(\boldsymbol{p})\end{pmatrix} + 16\alpha^2 \begin{pmatrix}\partial_{p_1} g^{(2)}(\boldsymbol{p}) \\ \partial_{p_2} g^{(2)}(\boldsymbol{p}) \\ \partial_{p_3} g^{(2)}(\boldsymbol{p})\end{pmatrix}\right), \tag{2.16}$$

in which ∇_p is the gradient with respect to $\boldsymbol{p}$, and the expansions of $\partial_{p_i} g^{(j)}$, $i = 1, 2, 3$, $j = 1, 2$, could be obtained in (2.4) and (2.5).

3 | THE PROPOSED NUMERICAL SCHEME

3.1 | Fourier pseudo-spectral spatial approximations

In comparison with the standard Fourier spectral method, the Fourier pseudo-spectral method (Fourier collocation spectral method) complements the basis by an additional pseudo-spectral basis, so that discrete functions are evaluated on the quadrature grid points. As a result, the computation of certain nonlinear operators, such as those involving point-wise products or quotients, can be considerably sped up, with the help of the fast Fourier transform (FFT). See the related descriptions in [3,8,15,17,18,21,29-31,38].

To simplify the notation, we set the domain as $\Omega = (0,1)^3$, with $N_x = N_y = N_z =: N \in \mathbb{N}$ and $N \cdot h = 1$, and $N = 2K + 1$, for some $K \in \mathbb{N}$. In fact, the analysis of an even integer N could be carried out in a similar manner, while more tedious details have to be included. All the physical variables are evaluated on the standard 3D numerical grid Ω_N, given by (x_i, y_j, z_k), with $x_i = ih$, $y_j = jh$, $z_k = kh$, $0 \le i, j, k \le 2K + 1$. In addition, the grid function space is denoted as

$$\mathcal{G}_N := \left\{f : \mathbb{Z}^3 \to \mathbb{R} \mid f \text{ is } \Omega_N\text{-periodic}\right\}. \tag{3.1}$$

For any $f \in \mathcal{G}_N$, its discrete Fourier expansion is given by

$$f_{i,j,k} = \sum_{\ell,m,n=-K}^{K} \hat{f}_{\ell,m,n}^N \exp(2\pi i(\ell x_i + m y_j + n z_k)), \tag{3.2}$$

where

$$\hat{f}_{\ell,m,n}^N := h^3 \sum_{i,j,k=0}^{N-1} f_{i,j,k} \exp(-2\pi i(\ell x_i + m x_j + n x_k)). \tag{3.3}$$

In turn, the collocation Fourier spectral first and second order derivatives of f turn out to be

$$\mathcal{D}_x f_{i,j,k} := \sum_{\ell,m,n=-K}^{K} (2\pi i\ell)\hat{f}_{\ell,m,n}^N \exp(2\pi i(\ell x_i + m y_j + n z_k)), \tag{3.4}$$

$$\mathcal{D}_x^2 f_{i,j,k} := \sum_{\ell,m,n=-K}^{K} (-4\pi^2\ell^2)\hat{f}_{\ell,m,n}^N \exp(2\pi i(\ell x_i + m y_j + n z_k)). \tag{3.5}$$

Similar definitions could be made for $\mathcal{D}_y$, $\mathcal{D}_y^2$, $\mathcal{D}_z$, and $\mathcal{D}_z^2$, the differentiation operators in the y and z directions, respectively. Of course, the discrete Laplacian, gradient and divergence operators become

$$\Delta_N f := \left(\mathcal{D}_x^2 + \mathcal{D}_y^2 + \mathcal{D}_z^2\right)f, \quad \nabla_N f := \begin{pmatrix} \mathcal{D}_x f \\ \mathcal{D}_y f \\ \mathcal{D}_z f \end{pmatrix}, \quad \nabla_N \cdot \begin{pmatrix} f_1 \\ f_2 \\ f_3 \end{pmatrix} := \mathcal{D}_x f_1 + \mathcal{D}_y f_2 + \mathcal{D}_z f_3, \tag{3.6}$$

at the point-wise level. It is obvious that $\nabla_N \cdot \nabla_N f = \Delta_N f$.

Detailed calculations show that the following summation-by-parts formulas are valid (see the related discussions in [11,13,30,31]):

$$\langle f, \Delta_N g \rangle = -\langle \nabla_N f, \nabla_N g \rangle, \quad \langle f, \Delta_N^2 g \rangle = \langle \Delta_N f, \Delta_N g \rangle, \quad \forall f, g \in \mathcal{G}_N. \tag{3.7}$$

Definition 3.1. Define $C_{\text{per}}(\Omega, \mathbb{R}) := \left\{ f : \Omega \to \mathbb{R} \mid \text{f is periodic and continuous on } \Omega \right\}$.
The grid projection $Q_N : C_{\text{per}}(\Omega, \mathbb{R}) \to \mathcal{G}_N$ is defined via

$$Q_N(g)_{i,j,k} := g(x_i, y_j, z_k). \tag{3.8}$$

The discrete ℓ^2 inner product and norm are defined as follows:

$$\langle f, g \rangle := h^3 \sum_{i,j,k=0}^{N-1} f_{i,j,k} \cdot g_{i,j,k}, \quad \|f\|_2 := \sqrt{\langle f, f \rangle}, \quad \forall f, g \in \mathcal{G}_N. \tag{3.9}$$

In particular, the zero-mean grid function subspace is denoted as $\mathring{\mathcal{G}}_N := \left\{ f \in \mathcal{G}_N \mid \langle f, 1 \rangle =: \bar{f} = 0 \right\}$. In addition to the standard ℓ^2 norm, we also introduce the ℓ^p, $1 \le p < \infty$, and ℓ^∞ norms for a grid function $f \in \mathcal{G}_N$:

$$\|f\|_\infty := \max_{i,j,k}|f_{i,j,k}|, \qquad \|f\|_p := \left(h^3 \sum_{i,j,k=0}^{N-1} |f_{i,j,k}|^p \right)^{\frac{1}{p}}, \quad 1 \le p < \infty. \tag{3.10}$$

For any periodic grid function $f \in \mathcal{G}_N$, the discrete H^1 and H^2 norms are given by

$$\|f\|_{H_N^1}^2 = \|f\|_2^2 + \|\nabla_N f\|_2^2, \quad \|f\|_{H_N^2}^2 = \|f\|_{H_N^1}^2 + \|\Delta_N f\|_2^2. \tag{3.11}$$

Since the anisotropic Equation (1.3) is an H^{-1} gradient flow, we need a discrete version of the $(\cdot, \cdot)_{H^{-1}}$ inner product and $\| \cdot \|_{H^{-1}}$ norm:

$$\langle f, g \rangle_{-1,N} := \langle f, (-\Delta_N)^{-1} g \rangle, \quad \|f\|_{-1,N} := \sqrt{\langle f, f \rangle_{-1,N}}, \quad \forall f, g \in \mathring{\mathcal{G}}_N. \tag{3.12}$$

For any $\phi \in \mathcal{G}_N$, the discrete energy for the PDE system (1.1) is defined as

$$E_N(\phi) := \frac{1}{4}\|\phi\|_4^4 - \frac{1}{2}\|\phi\|_2^2 + \frac{1}{4}|\Omega| + E_{S,N}(\phi) + \frac{\beta\varepsilon^2}{2}\|\Delta_N \phi\|_2^2, \tag{3.13}$$

where

$$E_{S,N}(\phi) := (1 - 3\alpha)^2 \|\nabla_N \phi\|_2 + E_{S,1,N}(\phi), \tag{3.14}$$

$$E_{S,1,N} := 8\alpha(1 - 3\alpha)\langle g^{(1)}(\nabla_N \phi), 1 \rangle + 16\alpha^2 \langle g^{(2)}(\nabla_N \phi), 1 \rangle. \tag{3.15}$$

Similarly, the following quantity is introduced

$$H_{2,N}(\phi) := A_2 \|\nabla_N \phi\|_2^2 - E_{S,1,N}(\phi), \tag{3.16}$$

so that the discrete energy functional could be rewritten as

$$E_N(\phi) = \langle f(\phi), \mathbf{1} \rangle + \frac{\varepsilon^2}{2} \left[(1 - 3\alpha)^2 + A_2 \right] \|\nabla_N \phi\|_2^2 - \frac{\varepsilon^2}{2} H_{2,N}(\phi) + \frac{\beta \varepsilon^2}{2} \|\Delta_N \phi\|_2^2. \tag{3.17}$$

Similar to the proof of Proposition 2.2, the following convexity result can be derived.

Proposition 3.2. *The functional $H_{2,N}(\phi)$ is convex, provided that (2.13) is satisfied.*

3.2 | The fully discrete numerical scheme and the theoretical results

We propose the following semi-implicit, second-order-in-time numerical scheme, with Fourier pseudo-spectral spatial approximation:

$$\frac{\frac{3}{2}\phi^{n+1} - 2\phi^n + \phi^{n-1}}{s} = \Delta_N \mu^{n+1}, \tag{3.18}$$

$$\begin{aligned} \mu^{n+1} = {} & (\phi^{n+1})^3 - (2\phi^n - \phi^{n-1}) - (1 - 3\alpha)^2 \varepsilon^2 \Delta_N \phi^{n+1} - As\Delta_N(\phi^{n+1} - \phi^n) + \beta\varepsilon^2 \Delta_N^2 \phi^{n+1} \\ & - 2\varepsilon^2 \nabla_N \cdot \left(4\alpha(1 - 3\alpha)\nabla_p g^{(1)}(\nabla_N \phi^n) + 8\alpha^2 \nabla_p g^{(2)}(\nabla_N \phi^n) \right) \\ & + \varepsilon^2 \nabla_N \cdot \left(4\alpha(1 - 3\alpha)\nabla_p g^{(1)}(\nabla_N \phi^{n-1}) + 8\alpha^2 \nabla_p g^{(2)}(\nabla_N \phi^{n-1}) \right). \end{aligned} \tag{3.19}$$

The following theoretical result of unique solvability and energy stability is available.

Theorem 3.3. *Given $\phi^n, \phi^{n-1} \in \mathcal{G}_N$ with $\overline{\phi^n} = \overline{\phi^{n-1}}$, for any $s > 0$, there exists a unique solution $\phi^{n+1} \in \mathcal{G}_N$ to the numerical scheme (3.18) and (3.19) satisfying the mass conservation condition: $\overline{\phi^{n+1}} = \overline{\phi^n} = \overline{\phi^{n-1}}$. Furthermore, provided that*

$$A \geq \max \left\{ \frac{1}{16}, \ \frac{1}{4}\left(\frac{1}{2} + \frac{1}{8\beta} \left[3A_2^\star - (1 - 3\alpha)^2 \right]^2 \varepsilon^2 \right)^2 \right\}, \tag{3.20}$$

the scheme is modified-energy stable, in the sense that, $\mathcal{E}_N(\phi^{n+1}, \phi^n) \leq \mathcal{E}_N(\phi^n, \phi^{n-1})$, where the modified energy functional is defined as

$$\mathcal{E}_N(\phi, \psi) := E_N(\phi) + \frac{1}{4s}\|\phi - \psi\|_{-1,N}^2 + \frac{A_2^\star \varepsilon^2}{2}\|\nabla_N(\phi - \psi)\|_2^2 + \frac{1}{2}\|\phi - \psi\|_2^2, \tag{3.21}$$

for all $\phi, \psi \in \mathcal{G}_N$ satisfying $\overline{\phi} = \overline{\psi}$.

Proof. Suppose that $\phi^n, \phi^{n-1} \in \mathcal{G}_N$ are given, with $\overline{\phi^n} = \overline{\phi^{n-1}}$. We observe that (3.18) and (3.19) can be rewritten as the solution of the following equation:

$$\mathcal{N}_N(\phi) = q^n, \tag{3.22}$$

where

$$\begin{aligned} \mathcal{N}_N(\phi) := {} & \frac{1}{s}(-\Delta_N)^{-1}\left(\frac{3}{2}\phi - 2\phi^n + \frac{1}{2}\phi^{n-1} \right) + \phi^3 - \left((1 - 3\alpha)^2\varepsilon^2 + As \right)\Delta_N \phi + \beta\varepsilon^2 \Delta_N^2 \phi, \\ q^n := {} & 2\phi^n - \phi^{n-1} - As\Delta_N\phi^n + 2\varepsilon^2\nabla_N \cdot \left(4\alpha(1 - 3\alpha)\nabla_p g^{(1)}(\nabla_N \phi^n) + 8\alpha^2\nabla_p g^{(2)}(\nabla_N \phi^n) \right) \\ & - \varepsilon^2\nabla_N \cdot \left(4\alpha(1 - 3\alpha)\nabla_p g^{(1)}(\nabla_N \phi^{n-1}) + 8\alpha^2\nabla_p g^{(2)}(\nabla_N \phi^{n-1}) \right). \end{aligned}$$

Of course, $\phi \in \mathcal{G}_N$ and the mass conservation condition, $\overline{\phi^{n+1}} = \overline{\phi^n} = \overline{\phi^{n-1}}$, is required. Since $\mathcal{N}_N(\phi) - q^n$ is the gradient of a strictly convex functional, namely,

$$J(\phi) = \frac{1}{3s}\left\|\frac{3}{2}\phi - 2\phi^n + \frac{1}{2}\phi^{n-1}\right\|_{-1,N}^2 + \frac{1}{4}\|\phi\|_4^4$$
$$+ \frac{1}{2}((1-3\alpha)^2\varepsilon^2 + As)\|\nabla_N\phi\|_2^2 + \frac{\beta\varepsilon^2}{2}\|\Delta_N\phi\|_2^2 - \langle q^n, \phi\rangle, \quad (3.23)$$

the unique solvability of (3.18) and (3.19) comes from a standard convexity analysis.

To obtain the energy stability analysis, a discrete inner product with (3.18) by $(-\Delta_N)^{-1}(\phi^{n+1} - \phi^n)$ is needed. An application of summation-by-parts yields

$$0 = \langle(\phi^{n+1})^3, \phi^{n+1} - \phi^n\rangle - \langle 2\phi^n - \phi^{n-1}, \phi^{n+1} - \phi^n\rangle - (1-3\alpha)^2\varepsilon^2\langle\Delta_N\phi^{n+1}, \phi^{n+1} - \phi^n\rangle$$
$$+ \beta\varepsilon^2\langle\Delta_N^2\phi^{n+1}, \phi^{n+1} - \phi^n\rangle - As\langle\Delta_N(\phi^{n+1} - \phi^n), \phi^{n+1} - \phi^n\rangle$$
$$+ \frac{1}{s}\left\langle\frac{3}{2}\phi^{n+1} - 2\phi^n + \frac{1}{2}\phi^{n-1}, (-\Delta_N)^{-1}(\phi^{n+1} - \phi^n)\right\rangle$$
$$- \varepsilon^2\langle\nabla_N \cdot \left(4\alpha(1-3\alpha)\nabla_p g^{(1)}(\nabla_N\phi^n) + 8\alpha^2\nabla_p g^{(2)}(\nabla_N\phi^n)\right), \phi^{n+1} - \phi^n\rangle$$
$$- 4\alpha(1-3\alpha)\varepsilon^2\langle\nabla_N \cdot \left(\nabla_p g^{(1)}(\nabla_N\phi^n) - \nabla_p g^{(1)}(\nabla_N\phi^{n-1})\right), \phi^{n+1} - \phi^n\rangle$$
$$- 8\alpha^2\varepsilon^2\langle\nabla_N \cdot \left(\nabla_p g^{(2)}(\nabla_N\phi^n) - \nabla_p g^{(2)}(\nabla_N\phi^{n-1})\right), \phi^{n+1} - \phi^n\rangle. \quad (3.24)$$

The following convexity estimates and identities are valid:

$$\langle(\phi^{n+1})^3, \phi^{n+1} - \phi^n\rangle \geq \frac{1}{4}\left\|\phi^{n+1}\right\|_4^4 - \frac{1}{4}\|\phi^n\|_4^4, \quad (3.25)$$

$$-\langle 2\phi^n - \phi^{n-1}, \phi^{n+1} - \phi^n\rangle \geq -\frac{1}{2}\left(\left\|\phi^{n+1}\right\|_2^2 - \|\phi^n\|_2^2\right) - \frac{1}{2}\left\|\phi^n - \phi^{n-1}\right\|_2^2, \quad (3.26)$$

$$-\langle\Delta_N\phi^{n+1}, \phi^{n+1} - \phi^n\rangle = \frac{1}{2}\left(\left\|\nabla_N\phi^{n+1}\right\|_2^2 - \left\|\nabla_N\phi^n\right\|_2^2\right) + \frac{1}{2}\left\|\nabla_N(\phi^{n+1} - \phi^n)\right\|_2^2, \quad (3.27)$$

$$-\langle\Delta_N(\phi^{n+1} - \phi^n), \phi^{n+1} - \phi^n\rangle = \left\|\nabla_N(\phi^{n+1} - \phi^n)\right\|_2^2. \quad (3.28)$$

For the BDF2 temporal stencil term, the following inequality can be derived:

$$I_1 := \frac{1}{s}\left\langle\frac{3}{2}\phi^{n+1} - 2\phi^n + \frac{1}{2}\phi^{n-1}, (-\Delta_N)^{-1}(\phi^{n+1} - \phi^n)\right\rangle$$
$$= \frac{1}{s}\left\langle\frac{3}{2}(\phi^{n+1} - \phi^n) - \frac{1}{2}(\phi^n - \phi^{n-1}), (-\Delta_N)^{-1}(\phi^{n+1} - \phi^n)\right\rangle_{-1,N}$$
$$= \frac{3}{2s}\|\phi^{n+1} - \phi^n\|_{-1,N}^2 - \frac{1}{2s}\langle\phi^n - \phi^{n-1}, (-\Delta_N)^{-1}(\phi^{n+1} - \phi^n)\rangle_{-1,N}$$
$$\geq \frac{3}{2s}\|\phi^{n+1} - \phi^n\|_{-1,N}^2 - \frac{1}{4s}(\|\phi^n - \phi^{n-1}\|_{-1,N}^2 + \|\phi^{n+1} - \phi^n\|_{-1,N}^2)$$
$$\geq \frac{1}{s}\left(\frac{5}{4}\left\|\phi^{n+1} - \phi^n\right\|_{-1,N}^2 - \frac{1}{4}\left\|\phi^n - \phi^{n-1}\right\|_{-1,N}^2\right), \quad (3.29)$$

in which the H^{-1} inner product and $\|\cdot\|_{-1,N}$ norm (3.12) have been utilized. The rest of our work will be focused on the nonlinear surface diffusion terms. The convexity property of the discrete quantity $H_{2,N}$ (given by Proposition 3.2) reveals that

$$-\langle\delta_\phi H_{2,N}(\phi^n), \phi^{n+1} - \phi^n\rangle \geq -(H_{2,N}(\phi^{n+1}) - H_{2,N}(\phi^n)). \quad (3.30)$$

Furthermore,

$$
\begin{aligned}
I_2 := &-\langle \nabla_N \cdot \left(8\alpha(1-3\alpha)\nabla_p g^{(1)}(\nabla_N \phi^n) + 16\alpha^2 \nabla_p g^{(2)}(\nabla_N \phi^n)\right), \phi^{n+1} - \phi^n \rangle \\
&+ 2A_2^\star \langle \Delta_N \phi^n, \phi^{n+1} - \phi^n \rangle \\
\geq &\, E_{S,1,N}(\phi^{n+1}) - E_{S,1,N}(\phi^n) - A_2^\star (\|\nabla_N \phi^{n+1}\|_2^2 - \|\nabla_N \phi^n\|_2^2).
\end{aligned}
\tag{3.31}
$$

On the other hand, the following identity is always valid

$$
2A_2^\star \langle \Delta \phi^n, \phi^{n+1} - \phi^n \rangle = -A_2^\star (\|\nabla_N \phi^{n+1}\|_2^2 - \|\nabla_N \phi^n\|_2^2) + A_2^\star \|\nabla_N(\phi^{n+1} - \phi^n)\|_2^2,
\tag{3.32}
$$

which in turn implies that

$$
\begin{aligned}
I_3 := &-\langle \nabla_N \cdot \left(8\alpha(1-3\alpha)\nabla_p g^{(1)}(\nabla_N \phi^n) + 16\alpha^2 \nabla_p g^{(2)}(\nabla_N \phi^n)\right), \phi^{n+1} - \phi^n \rangle \\
\geq &\, E_{S,1,N}(\phi^{n+1}) - E_{S,1,N}(\phi^n) - A_2^\star \|\nabla_N(\phi^{n+1} - \phi^n)\|_2^2.
\end{aligned}
\tag{3.33}
$$

For the last two terms associated with the nonlinear surface diffusion, we have to evaluate the difference of $\nabla_p g^{(i)}(\nabla_N \phi)$ between time steps t^n and t^{n-1}, for $i = 1, 2$, respectively. In more details, the first part could be expanded as

$$
\begin{aligned}
I_4 := &\langle \nabla_N \cdot \left(\nabla_p g^{(1)}(\nabla_N \phi^n) - \nabla_p g^{(1)}(\nabla_N \phi^{n-1})\right), \phi^{n+1} - \phi^n \rangle \\
= &-\langle \nabla_p g^{(1)}(\nabla_N \phi^n) - \nabla_p g^{(1)}(\nabla_N \phi^{n-1}), \nabla_N(\phi^{n+1} - \phi^n) \rangle \\
= &-\langle \partial_{p_1} g^{(1)}(\boldsymbol{p}^n) - \partial_{p_1} g^{(1)}(\boldsymbol{p}^{n-1}), p_1^{n+1} - p_1^n \rangle \\
&-\langle \partial_{p_2} g^{(1)}(\boldsymbol{p}^n) - \partial_{p_2} g^{(1)}(\boldsymbol{p}^{n-1}), p_2^{n+1} - p_2^n \rangle \\
&-\langle \partial_{p_3} g^{(1)}(\boldsymbol{p}^n) - \partial_{p_3} g^{(1)}(\boldsymbol{p}^{n-1}), p_3^{n+1} - p_3^n \rangle,
\end{aligned}
\tag{3.34}
$$

in which we have introduced the notation $\boldsymbol{p}^k = (p_1^k, p_2^k, p_3^k)^T = \nabla_N \phi^k = (\mathcal{D}_x \phi^k, \mathcal{D}_y \phi^k, \mathcal{D}_z \phi^k)^T$, $n - 1 \leq k \leq n + 1$, for simplicity of presentation. For the first expansion term, we apply (2.8) (from Lemma 2.1) and get

$$
|\partial_{p_1} g^{(1)}(\boldsymbol{p}^n) - \partial_{p_1} g^{(1)}(\boldsymbol{p}^{n-1})| \leq D_1^{(1)} |p_1^n - p_1^{n-1}| + D_2^{(1)} \left(|p_2^n - p_2^{n-1}| + |p_3^n - p_3^{n-1}|\right),
\tag{3.35}
$$

at a point-wise level. A summation in space implies that

$$
\begin{aligned}
I_{4,1} := &\left| \langle \partial_{p_1} g^{(1)}(\boldsymbol{p}^n) - \partial_{p_1} g^{(1)}(\boldsymbol{p}^{n-1}), p_1^{n+1} - p_1^n \rangle \right| \\
\leq &\frac{D_1^{(1)}}{2} \left(\left\| p_1^{n+1} - p_1^n \right\|_2^2 + \left\| p_1^n - p_1^{n-1} \right\|_2^2 \right) \\
&+ \frac{D_2^{(1)}}{2} \left(\left\| p_2^n - p_2^{n-1} \right\|_2^2 + \|p_3^n - p_3^{n-1}\|_2^2 + 2 \left\| p_1^{n+1} - p_1^n \right\|_2^2 \right).
\end{aligned}
\tag{3.36}
$$

The bounds for the two other nonlinear expansion terms could be similarly derived:

$$
\begin{aligned}
I_{4,2} := &\left| \langle \partial_{p_2} g^{(1)}(\boldsymbol{p}^n) - \partial_{p_2} g^{(1)}(\boldsymbol{p}^{n-1}), p_2^{n+1} - p_2^n \rangle \right| \\
\leq &\frac{D_1^{(1)}}{2} \left(\left\| p_2^{n+1} - p_2^n \right\|_2^2 + \left\| p_2^n - p_2^{n-1} \right\|_2^2 \right) \\
&+ \frac{D_2^{(1)}}{2} \left(\left\| p_1^n - p_1^{n-1} \right\|_2^2 + \|p_3^n - p_3^{n-1}\|_2^2 + 2 \left\| p_2^{n+1} - p_2^n \right\|_2^2 \right),
\end{aligned}
\tag{3.37}
$$

and

$$I_{4,3} := \left| \langle \partial_{p_3} g^{(1)}(\boldsymbol{p}^n) - \partial_{p_3} g^{(1)}(\boldsymbol{p}^{n-1}), p_3^{n+1} - p_3^n \rangle \right|$$

$$\leq \frac{D_1^{(1)}}{2} \left(\left\| p_3^{n+1} - p_3^n \right\|_2^2 + \left\| p_3^n - p_3^{n-1} \right\|_2^2 \right)$$

$$+ \frac{D_2^{(1)}}{2} \left(\left\| p_1^n - p_1^{n-1} \right\|_2^2 + \| p_2^n - p_2^{n-1} \|_2^2 + 2 \left\| p_3^{n+1} - p_3^n \right\|_2^2 \right). \tag{3.38}$$

A combination of (3.36)–(3.38) leads to

$$I_4 = \langle \nabla_N \cdot \left(\nabla_p g^{(1)}(\nabla_N \phi^n) - \nabla_p g^{(1)}(\nabla_N \phi^{n-1}) \right), \phi^{n+1} - \phi^n \rangle$$

$$\leq \frac{D_1^{(1)}}{2} \left(\left\| \nabla_N(\phi^{n+1} - \phi^n) \right\|_2^2 + \left\| \nabla_N(\phi^n - \phi^{n-1}) \right\|_2^2 \right)$$

$$+ D_2^{(1)} \left(\left\| \nabla_N(\phi^{n+1} - \phi^n) \right\|_2^2 + \left\| \nabla_N(\phi^n - \phi^{n-1}) \right\|^2 \right)$$

$$= \frac{B_0}{2} \left(\left\| \nabla_N(\phi^{n+1} - \phi^n) \right\|_2^2 + \left\| \nabla_N(\phi^n - \phi^{n-1}) \right\|_2^2 \right), \tag{3.39}$$

since

$$B_0 = D_1^{(1)} + 2 D_2^{(1)}.$$

The other nonlinear surface diffusion term can be analyzed in the same fashion, with the help of inequality (2.8) in Lemma 2.1:

$$I_5 := \left| \langle \nabla_N \cdot \left(\nabla_p g^{(2)}(\nabla_N \phi^n) - \nabla_p g^{(2)}(\nabla_N \phi^{n-1}) \right), \phi^{n+1} - \phi^n \rangle \right|$$

$$\leq \frac{A_0}{2} \left(\left\| \nabla(\phi^{n+1} - \phi^n) \right\|_2^2 + \left\| \nabla(\phi^n - \phi^{n-1}) \right\|_2^2 \right). \tag{3.40}$$

For the bi-harmonic regularization term, the following equality is available:

$$\langle \Delta_N^2 \phi^{n+1}, \phi^{n+1} - \phi^n \rangle = \frac{1}{2} (\| \Delta_N \phi^{n+1} \|^2 - \| \Delta_N \phi^n \|^2 + \| \Delta(\phi_N^{n+1} - \phi^n) \|^2). \tag{3.41}$$

A substitution of all these estimates into (3.24) leads to

$$0 \geq \frac{1}{4} (\| \phi^{n+1} \|_4^4 - \| \phi^n \|_4^4) - \frac{1}{2} (\| \phi^{n+1} \|_2^2 - \| \phi^n \|_2^2) + \frac{(1-3\alpha)^2 \varepsilon^2}{2} (\| \nabla_N \phi^{n+1} \|_2^2 - \| \nabla_N \phi^n \|_2^2)$$

$$+ \frac{\varepsilon^2}{2} \left(E_{S,1,N}(\phi^{n+1}) - E_{S,1,N}(\phi^n) \right) - \frac{1}{2} \| \phi^n - \phi^{n-1} \|_2^2$$

$$+ \frac{\beta \varepsilon^2}{2} \left(\| \Delta_N \phi^{n+1} \|_2^2 - \| \Delta_N \phi^n \|^2 + \| \Delta_N(\phi^{n+1} - \phi^n) \|_2^2 \right)$$

$$+ \left(\frac{(1-3\alpha)^2}{2} - A_2^\star \right) \varepsilon^2 \| \nabla_N(\phi^{n+1} - \phi^n) \|_2^2 - \frac{A_2^\star \varepsilon^2}{2} \| \nabla_N(\phi^n - \phi^{n-1}) \|_2^2$$

$$+ \frac{1}{s} \left(\frac{5}{4} \left\| \phi^{n+1} - \phi^n \right\|_{-1,N}^2 - \frac{1}{4} \left\| \phi^n - \phi^{n-1} \right\|_{-1,N}^2 \right) + As \| \nabla_N(\phi^{n+1} - \phi^n) \|_2^2. \tag{3.42}$$

Meanwhile, an application of the Cauchy inequality reveals that

$$\frac{1}{s} \left\| \phi^{n+1} - \phi^n \right\|_{-1,N}^2 + As \left\| \nabla_N(\phi^{n+1} - \phi^n) \right\|_2^2 \geq 2\sqrt{A} \left\| \phi^{n+1} - \phi^n \right\|_2^2. \tag{3.43}$$

Inserting this estimate, we have

$$
\begin{aligned}
0 \geq &\ \frac{1}{4}(\|\phi^{n+1}\|_4^4 - \|\phi^n\|_4^4) - \frac{1}{2}(\|\phi^{n+1}\|_2^2 - \|\phi^n\|_2^2) + \frac{(1-3\alpha)^2 \varepsilon^2}{2}(\|\nabla_N \phi^{n+1}\|_2^2 - \|\nabla_N \phi^n\|_2^2) \\
&+ \frac{\varepsilon^2}{2}(E_{S,1,N}(\phi^{n+1}) - E_{S,1,N}(\phi^n)) + \frac{1}{4s}\left(\left\|\phi^{n+1} - \phi^n\right\|_{-1,N}^2 - \left\|\phi^n - \phi^{n-1}\right\|_{-1,N}^2\right) \\
&+ \frac{\beta \varepsilon^2}{2}\left(\|\Delta_N \phi^{n+1}\|_2^2 - \|\Delta_N \phi^n\|_2^2\right) + \frac{\beta \varepsilon^2}{2}\|\Delta_N(\phi^{n+1} - \phi^n)\|_2^2 \\
&+ \left(\frac{(1-3\alpha)^2}{2} - \frac{3}{2}A_2^\star\right)\varepsilon^2 \|\nabla_N(\phi^{n+1} - \phi^n)\|_2^2 \\
&+ \frac{A_2^\star \varepsilon^2}{2}\left(\|\nabla_N(\phi^{n+1} - \phi^n)\|_2^2 - \|\nabla_N(\phi^n - \phi^{n-1})\|_2^2\right) \\
&+ \left(2\sqrt{A} - \frac{1}{2}\right)\|\phi^{n+1} - \phi^n\|_2^2 + \frac{1}{2}\left(\|\phi^{n+1} - \phi^n\|_2^2 - \|\phi^n - \phi^{n-1}\|_2^2\right).
\end{aligned}
\tag{3.44}
$$

Under the constraint (3.20) for A, we see that

$$
\begin{aligned}
I_6 :=&\ \frac{\beta \varepsilon^2}{2}\|\Delta_N(\phi^{n+1} - \phi^n)\|_2^2 + \left(2\sqrt{A} - \frac{1}{2}\right)\|\phi^{n+1} - \phi^n\|_2^2 \\
\geq&\ 2\varepsilon \sqrt{\frac{\beta}{2}\left(2\sqrt{A} - \frac{1}{2}\right)}\|\nabla_N(\phi^{n+1} - \phi^n)\|_2^2 \\
\geq&\ \left|\frac{(1-3\alpha)^2}{2} - \frac{3}{2}A_2^\star\right|\varepsilon^2 \|\nabla_N(\phi^{n+1} - \phi^n)\|_2^2.
\end{aligned}
\tag{3.45}
$$

In turn, the desired energy estimate is obtained:

$$
\mathcal{E}_N(\phi^{n+1}, \phi^n) - \mathcal{E}_N(\phi^n, \phi^{n-1}) \leq 0.
\tag{3.46}
$$

This finishes the proof of Theorem 3.3. ∎

Remark 3.4. For the strongly anisotropic flow, the energy stability has to rely on the bi-harmonic surface diffusion term. This is expected, since bi-harmonic regularization is required for well-posedness of the PDE. The constraint (3.20) for the artificial stabilization parameter A depends on both β and ε. In more detail, we observe that a smaller value of β and larger value of ε would lead to a larger value of A to satisfy the constraint.

In most practical computational examples, both β and ε are small parameters, of scale 10^{-2} to 10^{-3}. Extensive numerical experiments have demonstrated that selecting $A = O(1)$ is sufficient to ensure the energy stability in the simulations.

Remark 3.5. There have been extensive works related to second-order-accurate-in-time, energy stable numerical schemes for various gradient flows. Most of these numerical methods are based on the standard Crank–Nicolson temporal discretization with certain modifications; see the related works for the isotropic Cahn–Hilliard model [21,24,34], phase field crystal (PFC) equation and the modified phase field crystal (MPFC) equation [1,2,25,39]; epitaxial thin film growth models [13,17,48,52]; non-local gradient flow models [32,33]; phase field model coupled with fluid flow [12,23,35,36]; et cetera. In this approach, the unique solvability is established by the convexity argument or the monotonicity analysis, while the energy stability could be derived by an inner product with the numerical chemical potential.

Meanwhile, a few more recent works of the BDF2-type schemes have been reported for certain gradient flow models, such as Cahn–Hilliard [16,55], slope-selection thin film equation [28], square phase field crystal [19], in which the energy stability was theoretically established. Similar to this article, a Douglas-Dupont type regularization has to be

included in the numerical scheme, while a careful analysis reveals its energy stability at a modified level. Such a BDF2-type approach turns out to be a very robust numerical tool in the study of gradient flows.

4 | THE OPTIMAL RATE CONVERGENCE ANALYSIS

Let Φ be the exact periodic solution of the strongly anisotropic CH Equation (1.3). For the convenience of the convergence analysis, we also define $\Phi_N(\cdot, t) := \mathcal{P}_N\Phi(\cdot, t)$ as the (spatial) Fourier projection of the exact solution into the space

$$\mathcal{B}^K := \left\{ f \text{ is a trigonometric polynomial } \middle| \deg(f) \leq K \right\}, \quad N = 2K + 1.$$

In more details, suppose that Φ has the following Fourier series representation on Ω:

$$\Phi(x, y, z, t) = \sum_{k,l,m=-\infty}^{\infty} \widehat{\Phi}_{k,l,m}(t) e^{2\pi i(k\ x + l\ y + mz)},$$
$$\text{with} \quad \widehat{\Phi}_{k,l,m}(t) = \frac{1}{|\Omega|} \int_\Omega \Phi(x, y, z, t) e^{-2\pi i(k\ x + l\ y + mz)}\ dx\ dy\ dz. \tag{4.1}$$

The (finite Fourier) projection of Φ onto the space $\mathcal{B}^K$ is defined as

$$\Phi_N(x, y, z, t) := \mathcal{P}_N\Phi(x, y, z, t) := \sum_{k,l,m=-K}^{K} \widehat{\Phi}_{k,l,m}(t) e^{2\pi i(k\ x + l\ y + mz)}. \tag{4.2}$$

In turn, the initial data for the numerical scheme (3.18) and (3.19) could be taken as the grid projections of Φ_N at $t = 0$ and $t = s$;

$$\phi^0 = Q_N\Phi_N(\cdot, t = 0) \quad \text{and} \quad \phi^1 = Q_N\Phi_N(\cdot, t = s).$$

One advantage of this choice could be observed in the fact that, the $\|\cdot\|_{-1,N}$ norm is well defined for the error function between the numerical solution ϕ^n and the exact projection solution Φ_N, because

$$\langle \phi^k, 1 \rangle = \int_\Omega \Phi(\cdot, k \cdot s)\ d\mathbf{x}, \quad k = 0, 1.$$

If the initial data has sufficient regularity, the following regularity assumption is made for the exact solution:

$$\Phi \in \mathcal{R} := H^3\left(0, T; C^0_{\text{per}}(\Omega)\right) \cap H^2\left(0, T; C^6_{\text{per}}(\Omega)\right) \cap L^\infty\left(0, T; H^{m+6}_{\text{per}}(\Omega)\right), \quad \text{with}$$
$$C^k_{\text{per}}(\Omega) = \left\{ f \text{ is periodic on } \Omega\ \middle|\ f \in C^k(\Omega) \right\}, \quad H^k_{\text{per}}(\Omega) = \left\{ f \text{ is periodic on } \Omega\ \middle|\ f \in H^k(\Omega) \right\}. \tag{4.3}$$

Theorem 4.1. *Let Φ be the exact periodic solution with of the strongly anisotropic CH Equation (1.3), with the initial data $\Phi(0) = \phi_0 \in H^{m+6}_{\text{per}}(\Omega)$, and with the regularity class $\mathcal{R}$ given by (4.3). Suppose ϕ is the fully discrete numerical solution of (3.18) and (3.19). Then the following error estimate is valid*:

$$\|\Phi_N^n - \phi^n\|_{-1,N} + \left(\beta\varepsilon^2 s \sum_{k=0}^{n} \|\Delta_N(\Phi_N - \phi)\|_2^2 \right)^{1/2} \leq C(s^2 + h^m), \tag{4.4}$$

where the constant $C > 0$ is independent of s and h but depends on the exact solution.

Proof. A combination of Taylor expansion in time and Fourier projection estimate gives the following truncation error

$$
\begin{aligned}
\frac{\frac{3}{2}\Phi_N^{n+1} - 2\Phi_N^n + \frac{1}{2}\Phi_N^{n-1}}{s} = {} & \Delta_N\left((\Phi_N^{n+1})^3 - (2\Phi_N^n - \Phi_N^{n-1}) - (1-3\alpha)^2\varepsilon^2\Delta_N\Phi_N^{n+1} + \beta\varepsilon^2\Delta_N^2\Phi_N^{n+1}\right. \\
& - 2\varepsilon^2\nabla_N\cdot\left(4\alpha(1-3\alpha)\nabla_p g^{(1)}(\nabla_N\Phi_N^n) + 8\alpha^2\nabla_p g^{(2)}(\nabla_N\Phi_N^n)\right) \\
& + \varepsilon^2\nabla_N\cdot\left(4\alpha(1-3\alpha)\nabla_p g^{(1)}(\nabla_N\Phi^{n-1}) + 8\alpha^2\nabla_p g^{(2)}(\nabla\Phi^{n-1})\right) \\
& \left.- As\Delta_N(\Phi_N^{n+1} - \Phi_N^n)\right) + \tau^n,
\end{aligned}
\tag{4.5}
$$

with $\|\tau^n\| \le C(s^2 + h^m)$. The numerical error function is defined as

$$
e^k := \Phi_N^k - \phi^k, \quad \text{at a point-wise level.}
$$

Then, subtracting (3.18) and (3.19) from (4.5) yields

$$
\begin{aligned}
\frac{\frac{3}{2}e^{n+1} - 2e^n + \frac{1}{2}e^{n-1}}{s} = {} & \Delta_N\left(\left((\Phi_N^{n+1})^2 + \Phi_N^{n+1}\phi^{n+1} + (\phi^{n+1})^2\right)e^{n+1} - (2e^n - e^{n-1})\right. \\
& - (1-3\alpha)^2\varepsilon^2\Delta_N e^{n+1} + \beta\varepsilon^2\Delta_N^2 e^{n+1} - As\Delta_N(e^{n+1} - e^n) \\
& - 2\varepsilon^2\nabla_N\cdot\left(4\alpha(1-3\alpha)\left(\nabla_p g^{(1)}(\nabla_N\Phi^n) - \nabla_p g^{(1)}(\nabla_N\phi^n)\right)\right. \\
& + 8\alpha^2\left(\nabla_p g^{(2)}(\nabla_N\Phi^n) - \nabla_p g^{(2)}(\nabla_N\phi^n)\right)\right) \\
& + \varepsilon^2\nabla_N\cdot\left(4\alpha(1-3\alpha)\left(\nabla_p g^{(1)}(\nabla_N\Phi^{n-1}) - \nabla_p g^{(1)}(\nabla_N\phi^{n-1})\right)\right. \\
& \left.\left.+ 8\alpha^2\left(\nabla_p g^{(2)}(\nabla_N\Phi^{n-1}) - \nabla_p g^{(2)}(\nabla_N\phi^{n-1})\right)\right)\right) + \tau^n.
\end{aligned}
\tag{4.6}
$$

Since the exact solution to the PDE system (1.3) is mass conservative, we conclude that the projection solution Φ_N preserves the same property:

$$
\begin{aligned}
\int_\Omega \Phi_N(\mathbf{x}, t)\, d\mathbf{x} &= \int_\Omega \Phi(\mathbf{x}, t)\, d\mathbf{x} = \int_\Omega \Phi(\mathbf{x}, 0)\, d\mathbf{x} = \int_\Omega \Phi_N(\mathbf{x}, 0)\, d\mathbf{x}, \quad \forall\, t > 0, \\
\overline{\Phi_N^k} &= \int_\Omega \Phi_N(\mathbf{x}, t)\, d\mathbf{x} = \int_\Omega \Phi_N(\mathbf{x}, 0)\, d\mathbf{x} = \overline{\Phi_N^0}, \quad \forall\, k \ge 0,
\end{aligned}
\tag{4.7}
$$

in which the fact that $\Phi_N^k \in \mathcal{B}^K$ has been applied. Meanwhile, the numerical solution (3.18) and (3.19) is mass conservative at a discrete level, as proved in Theorem 3.3. These facts imply that the numerical error function has zero-mean, at a discrete level:

$$
\overline{e^k} = 0, \quad \text{that is,} \quad e^k \in \ddot{\mathcal{G}}_N, \quad \forall k \ge 0.
\tag{4.8}
$$

Subsequently, $\psi^k := (-\Delta_N)^{-1}e^k \in \ddot{\mathcal{G}}_N$ could be introduced. A discrete inner product with the error evolutionary Equation (4.6) by $2\psi^{n+1}$ leads to

$$
\begin{aligned}
& 2\left\langle \frac{3}{2}e^{n+1} - 2e^n + \frac{1}{2}e^{n-1}, (-\Delta_N)^{-1}e^{n+1}\right\rangle \\
& + 2(1-3\alpha)^2\varepsilon^2 s\|\nabla_N e^{n+1}\|_2^2 + 2\beta\varepsilon^2 s\|\Delta_N e^{n+1}\|_2^2 - 2A\varepsilon^2 s^2\langle\Delta_N(e^{n+1} - e^n), e^{n+1}\rangle \\
& = -2s\langle\left((\Phi_N^{n+1})^2 + \Phi_N^{n+1}\phi^{n+1} + (\phi^{n+1})^2\right)e^{n+1}, e^{n+1}\rangle + 2s\langle 2e^n - e^{n-1}, e^{n+1}\rangle \\
& \quad - 16\alpha(1-3\alpha)\varepsilon^2 s\langle\nabla_p g^{(1)}(\nabla_N\Phi_N^n) - \nabla_p g^{(1)}(\nabla_N\phi^n), \nabla_N e^{n+1}\rangle \\
& \quad - 32\alpha^2\varepsilon^2 s\langle\nabla_p g^{(2)}(\nabla_N\Phi_N^n) - \nabla_p g^{(2)}(\nabla_N\phi^n), \nabla_N e^{n+1}\rangle \\
& \quad + 8\alpha(1-3\alpha)\varepsilon^2 s\langle\nabla_p g^{(1)}(\nabla_N\Phi_N^{n-1}) - \nabla_p g^{(1)}(\nabla_N\phi^{n-1}), \nabla_N e^{n+1}\rangle \\
& \quad + 16\alpha^2\varepsilon^2 s\langle\nabla_p g^{(2)}(\nabla_N\Phi_N^{n-1}) - \nabla_p g^{(2)}(\nabla_N\phi^{n-1}), \nabla_N e^{n+1}\rangle + 2s\langle\tau^n, \psi^{n+1}\rangle.
\end{aligned}
\tag{4.9}
$$

The BDF2 temporal stencil term could be analyzed as follows:

$$
\begin{aligned}
& \left\langle \frac{3}{2}e^{n+1} - 2e^n + \frac{1}{2}e^{n-1}, (-\Delta_N)^{-1}e^{n+1}\right\rangle \\
& \quad = \left\langle \frac{3}{2}e^{n+1} - 2e^n + \frac{1}{2}e^{n-1}, e^{n+1}\right\rangle_{-1,N}
\end{aligned}
$$

$$= \frac{1}{4} \left(\|e^{n+1}\|_{-1,N}^2 - \|e^n\|_{-1,N}^2 + \|2e^{n+1} - e^n\|_{-1,N}^2 - \|2e^n - e^{n-1}\|_{-1,N}^2 \right.$$
$$\left. + \|e^{n+1} - 2e^n + e^{n-1}\|_{-1,N}^2 \right). \tag{4.10}$$

The bound for the truncation error term is standard:

$$\langle \tau^n, \psi^{n+1} \rangle \leq \|\tau^n\|_{-1,N} \cdot \|\nabla_N \psi^{n+1}\|_2 = \|\tau^n\|_{-1,N} \cdot \|e^{n+1}\|_{-1,N} \leq \frac{1}{2} \left(\|e^{n+1}\|_{-1,N}^2 + \|\tau^n\|_{-1,N}^2 \right). \tag{4.11}$$

For the last term on the left hand side of (4.9), the following inequality is available:

$$-\langle \Delta_N(e^{n+1} - e^n), e^{n+1} \rangle = \langle \nabla_N(e^{n+1} - e^n), \nabla_N e^{n+1} \rangle \geq \frac{1}{2} \left(\|\nabla_N e^{n+1}\|_2^2 - \|\nabla_N e^n\|_2^2 \right). \tag{4.12}$$

The first term on the right hand side always keeps non-positive:

$$-\langle \left((\Phi^{n+1})^2 + \Phi^{n+1} \phi^{n+1} + (\phi^{n+1})^2 \right) e^{n+1}, e^{n+1} \rangle \leq 0, \tag{4.13}$$

which comes from the fact that $(\Phi^{n+1})^2 + \Phi^{n+1} \phi^{n+1} + (\phi^{n+1})^2 \geq 0$. The Cauchy inequality could be applied to the concave expansive term:

$$\langle 2e^n - e^{n-1}, e^{n+1} \rangle \leq \frac{1}{2} \left(3\|e^{n+1}\|_2^2 + 2\|e^n\|_2^2 + \|e^{n-1}\|_2^2 \right)$$
$$\leq \frac{\varepsilon^2}{4} \left(3\|\nabla_N e^{n+1}\|_2^2 + 2\|\nabla_N e^n\|_2^2 + \|\nabla_N e^{n-1}\|_2^2 \right)$$
$$+ \frac{\varepsilon^{-2}}{4} \left(3\|e^{n+1}\|_{-1,N}^2 + 2\|e^n\|_{-1,N}^2 + \|e^{n-1}\|_{-1,N}^2 \right), \tag{4.14}$$

since $\quad \|e^k\|_2^2 \leq \|\nabla_N e^k\|_2 \cdot \|e^k\|_{-1,N} \leq \frac{\varepsilon^2}{2} \|\nabla_N e^k\|_2^2 + \frac{\varepsilon^{-2}}{2} \|e^k\|_{-1,N}^2, \quad k = n-1, n, n+1. \tag{4.15}$

The next few estimates are focused on the nonlinear error terms. At time step t^n, the following expansion is valid:

$$- \langle \nabla_p g^{(1)}(\nabla_N \Phi_N^n) - \nabla_p g^{(1)}(\nabla_N \phi^n), \nabla_N e^{n+1} \rangle$$
$$= -\langle \partial_{p_1} g^{(1)}(\nabla_N \Phi_N^n) - \partial_{p_1} g^{(1)}(\nabla_N \phi^n), \mathcal{D}_x e^{n+1} \rangle - \langle \partial_{p_2} g^{(1)}(\nabla_N \Phi_N^n) - \partial_{p_2} g^{(1)}(\nabla_N \phi^n), \mathcal{D}_y e^{n+1} \rangle$$
$$- \langle \partial_{p_3} g^{(1)}(\nabla_N \Phi_N^n) - \partial_{p_3} g^{(1)}(\nabla_N \phi^n), \mathcal{D}_z e^{n+1} \rangle. \tag{4.16}$$

For the first expansion term, we apply (2.8) from Lemma 2.1 and get

$$|\partial_{p_1} g^{(1)}(\nabla_N \Phi^n) - \partial_{p_1} g^{(1)}(\nabla_N \phi^n)| \leq D_1^{(1)} |\mathcal{D}_x e^n| + D_2^{(1)} \left(|\mathcal{D}_y e^n| + |\mathcal{D}_z e^n| \right), \tag{4.17}$$

at a point-wise level. This in turn implies that

$$\left| \langle \partial_{p_1} g^{(1)}(\nabla_N \Phi_N^n) - \partial_{p_1} g^{(1)}(\nabla_N \phi^n), \mathcal{D}_x e^{n+1} \rangle \right|$$
$$\leq \left(D_1^{(1)} \|\mathcal{D}_x e^n\|_2 + D_2^{(1)}(\|\mathcal{D}_y e^n\|_2 + \|\mathcal{D}_z e^n\|_2) \right) \|\mathcal{D}_x e^n\|_2$$
$$\leq \frac{D_1^{(1)}}{2} (\|\mathcal{D}_x e^n\|_2^2 + \|\mathcal{D}_x e^{n+1}\|_2^2) + \frac{D_2^{(1)}}{2} \left(\|\mathcal{D}_y e^n\|_2^2 + \|\mathcal{D}_2 e^n\|_2^2 + 2\|\mathcal{D}_x e^{n+1}\|_2^2 \right). \tag{4.18}$$

The bounds for the two other nonlinear expansion terms could be similarly derived:

$$\left| \langle \partial_{p_2} g^{(1)}(\nabla_N \Phi_N^n) - \partial_{p_2} g^{(1)}(\nabla_N \phi^n), \mathcal{D}_y e^{n+1} \rangle \right|$$
$$\leq \frac{D_1^{(1)}}{2} \left(\|\mathcal{D}_y e^n\|_2^2 + \|\mathcal{D}_x e^{n+1}\|_2^2 \right) + \frac{D_2^{(1)}}{2} \left(\|\mathcal{D}_x e^n\|_2^2 + \|\mathcal{D}_z e^n\|_2^2 + 2\|\mathcal{D}_y e^{n+1}\|_2^2 \right), \tag{4.19}$$

$$\left| \langle \partial_{p_3} g^{(1)}(\nabla_N \Phi_N^n) - \partial_{p_3} g^{(1)}(\nabla_N \phi^n), \mathcal{D}_z e^{n+1} \rangle \right|$$
$$\leq \frac{D_1^{(1)}}{2} \left(\|\mathcal{D}_z e^n\|_2^2 + \|\mathcal{D}_z e^{n+1}\|_2^2 \right) + \frac{D_2^{(1)}}{2} \left(\|\mathcal{D}_x e^n\|_2^2 + \|\mathcal{D}_y e^n\|_2^2 + 2\|\mathcal{D}_z e^{n+1}\|_2^2 \right). \tag{4.20}$$

A combination of (4.18)–(4.20) leads to

$$\left| \langle \nabla_p g^{(1)}(\nabla_N \Phi_N^n) - \nabla_p g^{(1)}(\nabla_N \phi^n), \nabla_N e^{n+1} \rangle \right| \leq \frac{D_1^{(1)}}{2} \left(\|\nabla_N e^n\|_2^2 + \|\nabla_N e^{n+1}\|_2^2 \right)$$
$$+ D_2^{(1)} \left(\|\nabla_N e^n\|_2^2 + \|\nabla_N e^{n+1}\|_2^2 \right)$$
$$= \frac{B_0}{2} \left(\|\nabla_N e^n\|_2^2 + \|\nabla_N e^{n+1}\|_2^2 \right), \tag{4.21}$$

in which the identity, $B_0 = D_1^{(1)} + 2D_2^{(1)}$, has been applied again.

The other nonlinear error term could be analyzed in the same fashion, with the help of inequality (2.8) in Lemma 2.1:

$$\left| \langle \nabla_p g^{(2)}(\nabla_N \Phi_N^n) - \nabla_p g^{(2)}(\nabla_N \phi^n), \nabla_N e^{n+1} \rangle \right| \leq \frac{A_0}{2} \left(\|\nabla_N e^n\|_2^2 + \|\nabla_N e^{n+1}\|_2^2 \right). \tag{4.22}$$

Likewise, the estimates for the nonlinear surface diffusion error terms at time step t^{n-1} are also available:

$$\left| \langle \nabla_p g^{(1)}(\nabla_N \Phi_N^{n-1}) - \nabla_p g^{(1)}(\nabla_N \phi^{n-1}), \nabla_N e^{n+1} \rangle \right| \leq \frac{B_0}{2} \left(\|\nabla_N e^{n-1}\|_2^2 + \|\nabla_N e^{n+1}\|_2^2 \right), \tag{4.23}$$

$$\left| \langle \nabla_p g^{(2)}(\nabla_N \Phi_N^{n-1}) - \nabla_p g^{(2)}(\nabla_N \phi^{n-1}), \nabla_N e^{n+1} \rangle \right| \leq \frac{A_0}{2} \left(\|\nabla_N e^{n-1}\|_2^2 + \|\nabla_N e^{n+1}\|_2^2 \right). \tag{4.24}$$

A substitution of all these inequalities into (4.9) yields

$$\frac{1}{2} \left(\|e^{n+1}\|_{-1,N}^2 - \|e^n\|_{-1,N}^2 + \|2e^{n+1} - e^n\|_{-1,N}^2 - \|2e^n - e^{n-1}\|_{-1,N}^2 \right)$$
$$+ 2\beta\varepsilon^2 s \|\Delta_N e^{n+1}\|_2^2 + As^2(\|\nabla_N e^{n+1}\|_2^2 - \|\nabla_N e^n\|_2^2)$$
$$\leq \varepsilon^2 s \left(\tilde{C}_1 \|\nabla_N e^{n+1}\|_2^2 + \tilde{C}_2 \|\nabla_N e^n\|_2^2 + \tilde{C}_3 \|\nabla_N e^{n-1}\|_2^2 \right)$$
$$+ \frac{\varepsilon^{-2}}{4} s \left(3\|e^{n+1}\|_{-1,N}^2 + 2\|e^n\|_{-1,N}^2 + \|e^{n-1}\|_{-1,N}^2 \right) + s(\|e^{n+1}\|_{-1,N}^2 + \|\tau^n\|_{-1,N}^2), \tag{4.25}$$

where

$$\tilde{C}_1 := \left| 2(1 - 3\alpha)^2 - 12\alpha|1 - 3\alpha|B_0 - 24\alpha^2 A_0 - \frac{3}{2} \right|,$$
$$\tilde{C}_2 := 8\alpha|1 - 3\alpha|B_0 + 16\alpha^2 A_0 + 1,$$
$$\tilde{C}_3 := 4\alpha|1 - 3\alpha|B_0 + 8\alpha^2 A_0 + \frac{1}{2}.$$

Meanwhile, based on the Sobolev interpolation inequality,

$$\|\nabla_N f\|_2 \leq \|f\|_{-1,N}^{1/3} \cdot \|\Delta_N f\|_2^{2/3},$$

we are able to apply Young's inequality and obtain

$$\tilde{C}_1 \|\nabla_N e^k\|_2^2 \leq \tilde{C}_1 \|e^k\|_{-1,N}^{2/3} \cdot \|\Delta_N e^k\|_2^{4/3} \leq \frac{\tilde{C}_1^3 \beta^{-2}}{3} \|e^k\|_{-1,N}^2 + \frac{\beta}{2} \|\Delta_N e^k\|_2^2, \tag{4.26}$$

for $k = n - 1$, n, and $n + 1$. Going back (4.25), we arrive at

$$
\frac{1}{2} \left(\|e^{n+1}\|_{-1,N}^2 - \|e^n\|_{-1,N}^2 + \|2e^{n+1} - e^n\|_{-1,N}^2 - \|2e^n - e^{n-1}\|_{-1,N}^2 \right)
$$

$$
+ As^2(\|\nabla_N e^{n+1}\|_2^2 - \|\nabla_N e^n\|_2^2) + \frac{3}{2}\beta\varepsilon^2 s\|\Delta_N e^{n+1}\|_2^2 - \frac{1}{2}\beta\varepsilon^2 s(\|\Delta_N e^n\|_2^2 + \|\Delta_N e^{n-1}\|_2^2)
$$

$$
\leq \frac{\beta^{-2}\varepsilon^2}{3} s \left(\tilde{C}_1^3 \|e^{n+1}\|_{-1,N}^2 + \tilde{C}_2^3 \|e^n\|_{-1,N}^2 + \tilde{C}_3^3 \|e^{n-1}\|_{-1,N}^2 \right)
$$

$$
+ \frac{\varepsilon^{-2}}{4} s \left(3\|e^{n+1}\|_{-1,N}^2 + 2\|e^n\|_{-1,N}^2 + \|e^{n-1}\|_{-1,N}^2 \right) + s(\|e^{n+1}\|_{-1,N}^2 + \|\tau^n\|_{-1,N}^2). \quad (4.27)
$$

Consequently, an application of a discrete Gronwall inequality leads to the desired convergence estimate of the numerical scheme (3.18) and (3.19), in the $\ell^\infty(0, T; H_N^{-1}) \cap \ell^2(0, T; H_N^2)$ norm: provided $s > 0$ is sufficiently small, there is a constant $C > 0$, independent of s and h, such that

$$
\|e^n\|_{-1,N}^2 + \frac{\beta\varepsilon^2}{2} s \sum_{k=0}^n \|\Delta_N e^k\|_2^2 \leq C(s^4 + h^{2m}), \quad (4.28)
$$

for any $n \in \mathbb{N}$ satisfying $n \cdot s \leq T$. The proof of Theorem 4.1 is finished. ∎

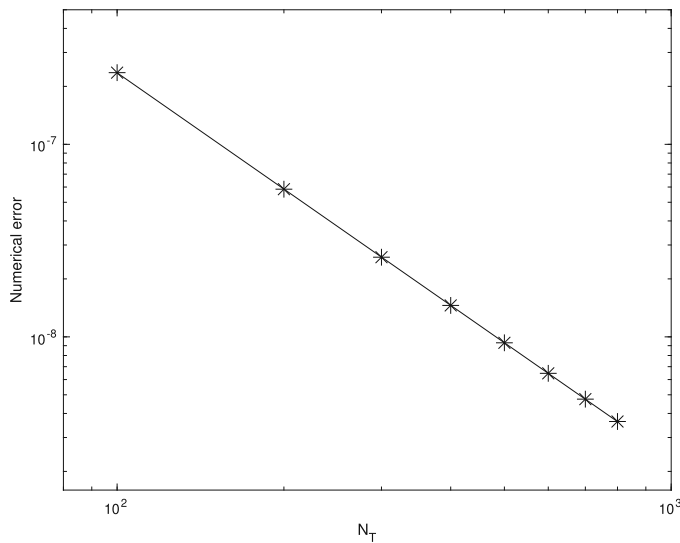## 5 | NUMERICAL RESULTS

5.1 | Convergence order test

Some numerical tests are performed to verify the convergence and accuracy order of the numerical scheme (3.18) and (3.19), for a sufficiently large anisotropy value $\alpha = 0.2$. The biharmonic regularization coefficient is taken as $\beta = 1$. In particular, one distinguished advantage of the proposed numerical scheme is associated with the explicit treatment for the nonlinear singular parts $g^{(1)}$ and $g^{(2)}$, which leads to a great improvement in terms of numerical efficiency, in comparison with an implicit computation. For the only nonlinear term in the numerical scheme, ϕ^3, we apply a preconditioned steepest descent (PSD) solver [27] for the detailed implement, because this nonlinear term corresponds to a strictly convex energy. The efficiency of the PSD solvers has been extensively demonstrated in quite a few recent works [19,28] to deal with non-singular gradient flow models.

In the convergence test, the exact solution for (1.3) is chosen as

$$
\phi_e(x, y, t) = \frac{1}{2\pi} \sin(2\pi x) \cos(2\pi y) \cos(t), \quad \text{over a square domain } \Omega = (0, 1)^2. \quad (5.1)
$$

The surface diffusion coefficient and the artificial diffusion coefficient are given by $\varepsilon = 0.05$, $A = \frac{1}{16}$, respectively, and we take the final time as $T = 1$.

Because of the spectral accuracy in space, the convergence test is focused on the temporal numerical error. We fix the spatial resolution as $N = 256$ so that the spatial numerical error is negligible. In turn, the solutions with a sequence of time step sizes: $s = \frac{T}{N_T}$ (with $N_T = 100$ to $N_T = 800$ in increments of 100), are computed with the final time $T = 1$. Figure 1 displays the discrete ℓ^2 norms of the errors between the numerical solution (3.18) and (3.19) and exact solution (1.3). In more details, the least square approximation to the CN_T^{-2} curve is displayed as the straight line in the figure, and a careful calculation gives an approximate value of the slope as -2.0062. Therefore, a perfect second order temporal accuracy is demonstrated in this experiment.

FIGURE 1 Discrete ℓ^2 numerical errors for the ϕ at the final time $T = 1$, plotted versus N_T, for the second order numerical scheme (3.18) and (3.19), with a fixed spatial resolution $N = 256$. The physical parameters: $\varepsilon = 0.05$, $\beta = 1$, $\alpha = 0.2$. The star line represents the numerical error plot versus N_T, while the straight line is the least square approximation to the CN_T^{-2} curve. The least square slope is calculated as -2.0062.

5.2 | Simulation results of four-fold-anisotropy

The numerical simulation is performed for the anisotropic Cahn–Hilliard system (1.3) over $\Omega = (0, 3.2)^2$, with the surface diffusion coefficient $\varepsilon = 0.03$ and anisotropic parameter $\alpha = 0.2$. The initial data are given by

$$\phi(x, y, t = 0) = -\tanh\left(\frac{(x - x_0)^2 + (y - y_0)^2 - r_0}{0.25\varepsilon}\right), \quad \text{with } x_0 = y_0 = 1.6, r_0 = 0.8. \tag{5.2}$$

In addition, the biharmonic regularization coefficient is chosen as $\beta = 0.0005$, and the artificial regularization parameter is taken to be $A = 4$. The temporal step size is given by $s = 10^{-3}$, and the spatial resolution is set as 512^2.
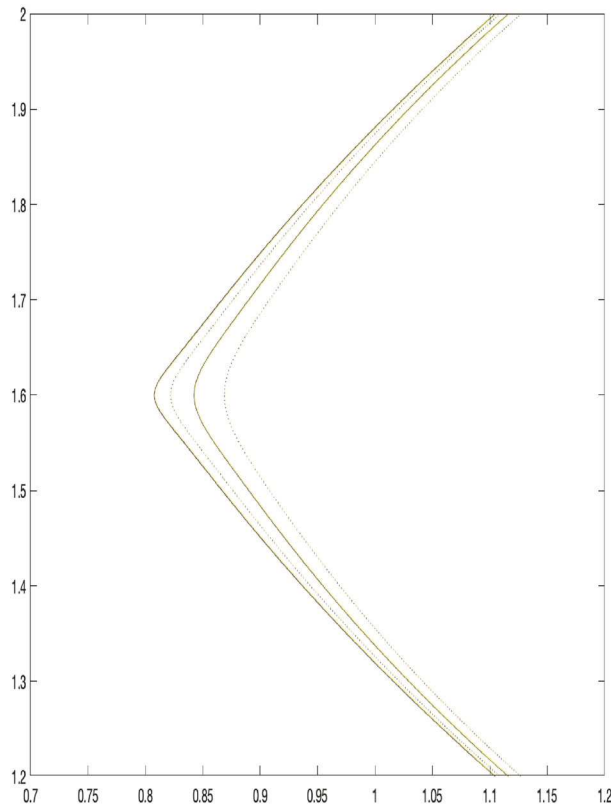
The time evolution snapshots of the phase variable computed by the second order numerical scheme (3.18) and (3.19) are displayed in Figure 2. The circular profile evolves to an anisotropic, four-fold shape with missing orientation at the four corners.

5.3 | Numerical comparison in terms of the biharmonic regularization parameter

The biharmonic regularization parameter β has always played an important role in the solution structure. For the two-dimensional, strongly anisotropic equation (1.3) with the initial data (5.2), we perform a numerical test by taking a sequence of parameters: $\beta = 0.004, 0.002, 0.001$, and 0.0005. The other physical parameters are taken the same as in Figure 2: $\varepsilon = 0.03, \Omega = (0, 3.2)^2$. At the final time $t = 30$, in which a steady state solution is reached, a comparison of the computational results around the left corner is presented in Figure 3. In fact, similar behaviors have also been reported in [14,20,54]; a smaller regularization coefficient always gives less corner rounding and a sharper profile.

$$t = 0.05 \qquad t = 0.1 \qquad t = 30.0$$

FIGURE 2 Time evolution snapshots of the phase variable at the time sequence: $t = 0.05, 0.1$, and 30. The physical parameters: $\alpha = 0.2, \beta = 0.0005, \varepsilon = 0.03, \Omega = (0, 3.2)^2$.

FIGURE 3 Comparison of the $\phi = 0.0$ iso-contour plots for numerical solutions obtained with four different corner regularization parameters, $\beta = 0.004, 0.002, 0.001$, and 0.0005, at the final time $t = 30$, with the initial data (5.2). The outer solid line, the outer dashed line, the inner solid line and the inner dashed line stand for the numerical solutions $\beta = 0.0005$, 0.001, 0.002, and 0.004, respectively. The physical parameters: $\varepsilon = 0.03, \Omega = (0, 3.2)^2$, and $\alpha = 0.2$.

5.4 | Simulation results of eight-fold-anisotropy

In this section, the numerical results of symmetric eight-fold-anisotropic function are presented; see the more detailed formulation of anisotropic function [14,44,49]

$$\gamma(\boldsymbol{n}) = 1 + \alpha \left(8 \sum_{i=1}^{d} \left(8n_i^8 - 10n_i^6 + n_i^4 \right) + 9 \right). \tag{5.3}$$

Again, the initial data (5.2) are taken, and the physical parameters are set as: $\varepsilon = 0.03$, $\alpha = 0.2$, $\beta = 0.002$, $s = 10^{-4}$. The time snapshots of the evolution computed by the second order numerical scheme (3.18) and (3.19), with spatial resolution 512^2, are presented in Figure 4. It is clear that an octagonal shape has emerges. In terms of a comparison the four-fold and eight-fold anisotropic gradient flows, which are presented in Figures 2 and 4, respectively, it is clear that the evolution dynamics is similar. An early structure is observed at $t = 0.05$, an intermediate time scale structure becomes closer to an anisotropic shape ($t = 0.1$ for the four-fold flow, $t = 1$ for the eight-fold flow), and a steady state structure is reported at $t = 30$.

5.5 | Three-dimensional simulation results

We present some three-dimensional numerical simulation results. Similarly, the four-fold anisotropic function (1.1) is taken, and the initial data are given by
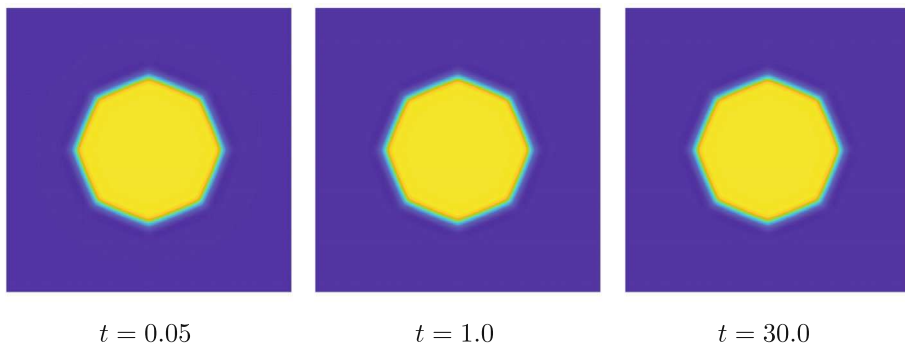

| $t = 0.05$ | $t = 1.0$ | $t = 30.0$ |

FIGURE 4 Time evolution snapshots of the phase variable at a time sequence: $t = 0.05, 1,$ and 30, with an eight-fold symmetric anisotropic function (5.3). The parameters are set as $\varepsilon = 0.03$, $\alpha = 0.2$, $\Omega = (0, 3.2)^2$.
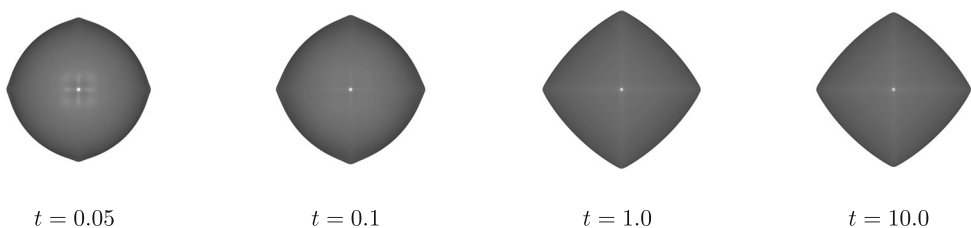

| $t = 0.05$ | $t = 0.1$ | $t = 1.0$ | $t = 10.0$ |

FIGURE 5 The surface plots of $\phi = 0$ for the 3-D anisotropic Cahn–Hilliard model at a time sequence: $t = 0.05, 0.1, 1,$ and 10. The four-fold symmetric anisotropic function is taken, as well as the initial data (5.4). The parameters are given by: $\varepsilon = 0.03$, $\alpha = 0.2$, $\Omega = (0, 3.2)^3$.

$$\phi(x, y, z, t = 0) = -\tanh\left(\frac{(x-x_0)^2 + (y-y_0)^2 + (z-z_0)^2 - r_0}{0.25\varepsilon}\right),$$
$$x_0 = y_0 = z_0 = 1.6, \quad r_0 = 0.8.$$

(5.4)

The physical parameters are set as: $\varepsilon = 0.03$, $\alpha = 0.2$, $\beta = 0.0005$, $s = 10^{-3}$. The surface plots of $\phi = 0$ for the numerical solution computed by the second numerical scheme (3.18) and (3.19), with spatial resolution 192^3, are presented in Figure 5.

6 | CONCLUDING REMARKS

A second order accurate in time, energy stable numerical scheme is proposed and analyzed for the strongly anisotropic Cahn–Hilliard model, with Fourier pseudo-spectral spatial approximation. A biharmonic regularization is included, to make the PDE system well-posed. A convexity analysis on the anisotropic interfacial energy is reviewed, based on the subtle fact that all its second order functional derivatives stay uniformly bounded by a global constant. Such a convexity analysis overcomes a well-known difficulty associated with the highly nonlinear and singular nature of the anisotropic surface energy, so that we are able to derive second order accurate numerical schemes while theoretically preserving the energy stability. In more details, the uniform bounds of the second order functional derivatives lead to an explicit extrapolation for the nonlinear surface energy part, and a Douglas-Dupont type regularization is added for the sake of numerical stability. A careful estimate ensures a modified energy dissipation property with a uniform constraint for the regularization parameter A. Its combination with an implicit treatment for the nonlinear double well potential term makes the numerical system weakly nonlinear. More importantly, the derived energy stability is in terms of the energy potential in the original phase variable, with no auxiliary variable included in the numerical scheme. In addition, an optimal rate convergence analysis and second order temporal error estimate are derived for the proposed numerical scheme, which is the first such result for the strongly anisotropic model.

A few numerical results have also been presented in this work, such as the convergence rate test, simulation results of four-fold and eight-fold anisotropic functions, numerical comparison between different biharmonic regularization parameters, et cetera.

DATA AVAILABILITY STATEMENT
The data that support the findings of this study are available from the corresponding author upon reasonable request.

ORCID
Steven M. Wise https://orcid.org/0000-0003-3824-2075

REFERENCES

[1] A. Baskaran, Z. Hu, J. Lowengrub, C. Wang, S. M. Wise, and P. Zhou, *Energy stable and efficient finite-difference nonlinear multigrid schemes for the modified phase field crystal equation*, J. Comput. Phys. 250 (2013), 270–292.

[2] A. Baskaran, J. Lowengrub, C. Wang, and S. Wise, *Convergence analysis of a second order convex splitting scheme for the modified phase field crystal equation*, SIAM J. Numer. Anal. 51 (2013), 2851–2873.

[3] J. Boyd, *Chebyshev and Fourier spectral methods*, Dover, New York, NY, 2001.

[4] M. Burger, F. Haußer, C. Stöcker, and A. Voigt, *A level set approach to anisotropic flows with curvature regularization*, J. Comput. Phys. 225 (2007), 183–205.

[5] J. W. Cahn, *On spinodal decomposition*, Acta Metall. 9 (1961), 795.

[6] J. W. Cahn and J. E. Hilliard, *Free energy of a nonuniform system. I. Interfacial free energy*, J. Chem. Phys. 28 (1958), 258–267.

[7] J. W. Cahn and D. W. Hoffman, *A vector thermodynamics for anisotropic surfaces-II, curved and faceted surfaces*, Acta Metall. 22 (1974), 1205–1214.

[8] C. Canuto and A. Quarteroni, *Approximation results for orthogonal polynomials in Sobolev spaces*, Math. Comp. 38 (1982), 67–86.

[9] C. Chen and X. Yang, *Fast, provably unconditionally energy stable, and second-order accurate algorithms for the anisotropic Cahn-Hilliard model*, Comput. Meth. Appl. Mech. Eng. 351 (2019), 35–59.

[10] F. Chen and J. Shen, *Efficient energy stable schemes with spectral discretization in space for anisotropic Cahn-Hilliard systems*, Commun. Comput. Phys. 13 (2013), 1189–1208.

[11] W. Chen, S. Conde, C. Wang, X. Wang, and S. M. Wise, *A linear energy stable scheme for a thin film model without slope selection*, J. Sci. Comput. 52 (2012), 546–562.

[12] W. Chen, W. Feng, Y. Liu, C. Wang, and S. M. Wise, *A second order energy stable scheme for the Cahn-Hilliard-Hele-Shaw equation*, Discrete Continuous Dyn. Syst. Ser. B 24 (2019), no. 1, 149–182.

[13] W. Chen, C. Wang, X. Wang, and S. M. Wise, *A linear iteration algorithm for energy stable second order scheme for a thin film model without slope selection*, J. Sci. Comput. 59 (2014), 574–601.

[14] Y. Chen, J. S. Lowengrub, J. Shen, C. Wang, and S. M. Wise, *Efficient energy stable schemes for isotropic and strongly anisotropic Cahn-Hilliard systems with the Willmore regularization*, J. Comput. Phys. 365 (2018), 57–73.

[15] K. Cheng, W. Feng, S. Gottlieb, and C. Wang, *A Fourier pseudospectral method for the "Good" Boussinesq equation with second-order temporal accuracy*, Numer. Methods Partial Differ. Equ. 31 (2015), no. 1, 202–224.

[16] K. Cheng, W. Feng, C. Wang, and S. M. Wise, *An energy stable fourth order finite difference scheme for the Cahn-Hilliard equation*, J. Comput. Appl. Math. 362 (2019), 574–595.

[17] K. Cheng, Z. Qiao, and C. Wang, *A third order exponential time differencing numerical scheme for no-slope-selection epitaxial thin film model with energy stability*, J. Sci. Comput. 81 (2019), no. 1, 154–185.

[18] K. Cheng and C. Wang, *Long time stability of high order multi-step numerical schemes for two-dimensional incompressible Navier-Stokes equations*, SIAM J. Numer. Anal. 54 (2016), 3123–3144.

[19] K. Cheng, C. Wang, and S. M. Wise, *An energy stable Fourier pseudo-spectral numerical scheme for the square phase field crystal equation*, Commun. Comput. Phys. 362 (2019), 574–595.

[20] K. Cheng, C. Wang, and S. M. Wise, *A weakly nonlinear energy stable scheme for the strongly anisotropic Cahn-Hilliard system and its convergence analysis*, J. Comput. Phys. 405 (2020), 109109.

[21] K. Cheng, C. Wang, S. M. Wise, and X. Yue, *A second-order, weakly energy-stable pseudo-spectral scheme for the Cahn-Hilliard equation and its solution by the homogeneous linear iteration method*, J. Sci. Comput. 69 (2016), 1083–1114.

[22] A. DiCarlo, M. Gurtin, and P. Podio-Guidugli, *A regularized equation for anisotropic motion-by-curvature*, SIAM J. Appl. Math. 52 (1992), 1111–1119.

[23] A. Diegel, C. Wang, X. Wang, and S. M. Wise, *Convergence analysis and error estimates for a second order accurate finite element method for the Cahn-Hilliard-Navier-Stokes system*, Numer. Math. 137 (2017), 495–534.

[24] A. Diegel, C. Wang, and S. M. Wise, *Stability and convergence of a second order mixed finite element method for the Cahn-Hilliard equation*, IMA J. Numer. Anal. 36 (2016), 1867–1897.

[25] L. Dong, W. Feng, C. Wang, S. M. Wise, and Z. Zhang, *Convergence analysis and numerical implementation of a second order numerical scheme for the three-dimensional phase field crystal equation*, Comput. Math. Appl. 75 (2018), no. 6, 1912–1928.

[26] J. J. Eggleston, G. B. McFadden, and P. W. Voorhees, *A phase-field model for highly anisotropic interfacial energy*, Physica D 150 (2001), 91–103.

[27] W. Feng, A. J. Salgado, C. Wang, and S. M. Wise, *Preconditioned steepest descent methods for some nonlinear elliptic equations involving p-Laplacian terms*, J. Comput. Phys. 334 (2017), 45–67.

[28] W. Feng, C. Wang, S. M. Wise, and Z. Zhang, *A second-order energy stable Backward Differentiation Formula method for the epitaxial thin film equation with slope selection*, Numer. Methods Partial Differ. Equ. 34 (2018), no. 6, 1975–2007.

[29] D. Gottlieb and S. A. Orszag, *Numerical analysis of spectral methods, theory and applications*, SIAM, Philadelphia, PA, 1977.

[30] S. Gottlieb, F. Tone, C. Wang, X. Wang, and D. Wirosoetisno, *Long time stability of a classical efficient scheme for two dimensional Navier-Stokes equations*, SIAM J. Numer. Anal. 50 (2012), 126–150.

[31] S. Gottlieb and C. Wang, *Stability and convergence analysis of fully discrete Fourier collocation spectral method for 3-D viscous Burgers' equation*, J. Sci. Comput. 53 (2012), 102–128.

[32] Z. Guan, J. S. Lowengrub, and C. Wang, *Convergence analysis for second order accurate schemes for the periodic nonlocal Allen-Cahn and Cahn-Hilliard equations*, Math. Methods Appl. Sci. 40 (2017), no. 18, 6836–6863.

[33] Z. Guan, J. S. Lowengrub, C. Wang, and S. M. Wise, *Second-order convex splitting schemes for nonlocal Cahn-Hilliard and Allen-Cahn equations*, J. Comput. Phys. 277 (2014), 48–71.

[34] J. Guo, C. Wang, S. M. Wise, and X. Yue, *An H^2 convergence of a second-order convex-splitting, finite difference scheme for the three-dimensional Cahn-Hilliard equation*, Commun. Math. Sci. 14 (2016), 489–515.

[35] D. Han, A. Brylev, X. Yang, and Z. Tan, *Numerical analysis of second order, fully discrete energy stable schemes for phase field models of two phase incompressible flows*, J. Sci. Comput. 70 (2017), no. 3, 965–989.

[36] D. Han and X. Wang, *A second order in time, uniquely solvable, unconditionally stable numerical scheme for Cahn-Hilliard-Navier-Stokes equation*, J. Comput. Phys. 290 (2015), 139–156.

[37] F. Hausser and A. Voigt, *A discrete scheme for regularized anisotropic surface diffusion: a 6th order geometric evolution equation*, Interface Free Bound 7 (2005), 353–369.

[38] J. Hesthaven, S. Gottlieb, and D. Gottlieb, *Spectral methods for time-dependent problems*, Cambridge University Press, Cambridge, UK, 2007.

[39] Z. Hu, S. Wise, C. Wang, and J. Lowengrub, *Stable and efficient finite-difference nonlinear-multigrid schemes for the phase-field crystal equation*, J. Comput. Phys. 228 (2009), 5323–5339.

[40] R. Kobayashi, *Modeling and numerical simulations of dendritic crystal growth*, Physica D 63 (1993), 410–423.

[41] A. Makki and A. Miranville, *Existence of solutions for anisotropic Cahn-Hilliard and Allen-Cahn systems in higher space dimensions*, Discrete Continuous Dyn. Syst. Ser. B 9 (2016), 759–775.

[42] A. Miranville, *Existence of solutions for a one-dimensional Allen-Cahn equation*, J. Appl. Anal. Comput. 12 (2013), 265–277.

[43] A. Rätz, A. Ribalta, and A. Voigt, *Surface evolution of elastically stressed films under deposition by a diffuse interface model*, J. Comput. Phys. 214 (2006), no. 1, 187–208.

[44] M. Salvalaglio, R. Backofen, R. Bergamaschini, F. Montalenti, and A. Voigt, *Faceting of equilibrium and metastable nanostructures: A phase-field model of surface diffusion tacking realistic shapes*, Cryst. Growth Des. 15 (2015), 2787–2794.

[45] M. Salvalaglio, R. Backofen, A. Voigt, and F. Montalenti, *Morphological evolution of pit-patterned Si(001) substrates driven by surface-energy reduction*, Nanoscale Res. Lett. 12 (2017), 554.

[46] M. Salvalaglio, A. Voigt, and S. M. Wise, *Doubly degenerate diffuse interface models of surface diffusion*, Math. Methods Appl. Sci. 44 (2021), no. 7, 5385–5405.

[47] R. F. Sekerka, *Analytical criteria for missing orientations on three-dimensional equilibrium shapes*, J. Cryst. Growth 275 (2005), 77–82.

[48] J. Shen, C. Wang, X. Wang, and S. M. Wise, *Second-order convex splitting schemes for gradient flows with Ehrlich-Schwoebel type energy: Application to thin film epitaxy*, SIAM J. Numer. Anal. 50 (2012), 105–125.

[49] E. J. Siem and W. C. Carter, *Orientation-dependent surface tension functions for surface energy minimizing calculations*, J. Mater. Sci. 40 (2005), 3107–3113.

[50] J. E. Taylor and J. W. Cahn, *Diffuse interface with sharp corners and facets: phase field models with strongly anisotropic surfaces*, Physica D 112 (1998), 381–411.

[51] S. Torabi, J. S. Lowengrub, A. Voigt, and S. M. Wise, *A new phase-field model for strongly anisotropic systems*, Proc. R. Soc. Lond. Ser. A Math. Phys. Eng. Sci. 465 (2009), 1337–1359.

[52] S. Wang, W. Chen, H. Pan, and C. Wang, *Optimal rate convergence analysis of a second order scheme for a thin film model with slope selection*, J. Comput. Appl. Math. 377 (2020), 112855.

[53] A. A. Wheeler, *Phase-field theory of edges in an anisotropic crystal*, Proc. R. Soc. A 462 (2006), 3363–3384.

[54] S. M. Wise, J. S. Kim, and J. S. Lowengrub, *Solving the regularized, strongly anisotropic Chan-Hilliard equation by an adaptive nonlinear multigrid method*, J. Comput. Phys. 226 (2007), 414–446.

[55] Y. Yan, W. Chen, C. Wang, and S. M. Wise, *A second-order energy stable BDF numerical scheme for the Cahn-Hilliard equation*, Commun. Comput. Phys. 23 (2018), 572–602.

[56] J. Zhang, C. Chen, X. Yang, Y. Chu, and Z. Xia, *Efficient, non-iterative, and second-order accurate numerical algorithms for the anisotropic Allen-Cahn equation with precise nonlocal mass conservation*, J. Comput. Appl. Math. 363 (2019), 444–463.